Arabian Journal of Chemistry (2023) **16**, 104683

King Saud University

Arabian Journal of Chemistry

www.ksu.edu.sa
www.sciencedirect.com

ORIGINAL ARTICLE

Optimization and mass transfer simulation of remazol brilliant blue R dye adsorption onto meranti wood based activated carbon

Mohamad Firdaus Mohamad Yusop [a], Muhammad Azan Tamar Jaya [b], Iylia Idris [c], Ahmad Zuhairi Abdullah [a], Mohd Azmier Ahmad [a,*]

[a] *School of Chemical Engineering, Engineering Campus, Universiti Sains Malaysia, 14300 Nibong Tebal, Penang, Malaysia*
[b] *Kolej GENIUS Insan, Universiti Sains Islam Malaysia, 71800 Nilai, Negeri Sembilan, Malaysia*
[c] *School of Chemical Engineering, College of Engineering, Universiti Teknologi MARA, 40450 Shah Alam, Selangor, Malaysia*

Received 1 December 2022; accepted 11 February 2023
Available online 15 February 2023

KEYWORDS

Activated carbon;
Adsorption process;
Response surface methodology;
Simulation;
Polymath;
Remazol brlilliant blue R

Abstract Remazol brilliant blue R dye (RBBR) brings toxicity to living organisms once it enters the environment. This study utilized response surface methodology (RSM) and Polymath software for optimization and mass transfer simulation purposes, respectively. RSM revealed that the optimum preparation conditions of meranti wood-based activated carbon (MWAC) were 441 W, 5.76 min, and 1.35 g/g for radiation power, radiation time, and KOH:char impregnation ratio (IR), respectively, which translated into 86.39 mg/g of RBBR uptakes and 31.94 % of MWAC's yield. The simulation study predicted the mass transfer rate, r_m to be 112.20 to 1007.50 s^{-1} and the adsorption rate, k_1 to be 3.96 to 4.34 h^{-1}. The developed model predicted the adsorption surface area, a_m to be 790.04 m^2/g and this value is highly accurate as compared to the actual mesopores surface area of 825.58 m^2/g. Mechanism analysis divulged that the interaction that occurred between RBBR molecules and MWAC's surface were hydrogen bond (methylene and alkyne), dipole–dipole force (alkyl carbonate, terminal alkyne, and methoxy), and ion–dipole force (primary amine). The isotherm and kinetic studies found that the adsorption data obeyed the Freundlich model and pseudo-first-order (PFO) model the best, respectively. The Langmuir maximum adsorption capacity, Q_m was computed to be 327.33 mg/g. Thermodynamic parameters were calculated to be −4.06 kJ mol^{-1}, 0.06 kJ mol^{-1} K^{-1}, –22.69 kJ mol^{-1}, and 16.03 kJ mol^{-1} for ΔH°, ΔS°, ΔG°, and E_a, respectively, which signified the adsorption process studied was exothermic, spontaneous

* Corresponding author.
E-mail address: chazmier@usm.my (M.A. Ahmad).
Peer review under responsibility of King Saud University.

Production and hosting by Elsevier

https://doi.org/10.1016/j.arabjc.2023.104683

and governed by physisorption.

1. Introduction

The annual production of synthetic dyes is kept rising due to the increasing demand worldwide. Several industries that extremely depend on synthetic dyes include textile, paper, magazines, cosmetics, and foods (Kishor et al., 2021). Synthetic dyes are a large group of organic chemicals and most of them contain complex aromatic in their structure. To date, almost 10,000 different types of synthetic dyes are reported in the literature (Firdaus et al., 2022). Based on their solubility in water, synthetic dyes can be divided into cationic (basic dyes), anionic (acid, direct, and reactive dyes), and non-ionic (vat and disperse dyes). Among them, reactive dyes are preferred to dye cotton due to their ability to attach to this material strongly. Unfortunately, reactive dyes may undergo hydrolysis during the dyeing process which prevents them from attaching to the textile substrate, thus producing highly polluted effluents of colours (Peláez-Cid et al., 2016). An example of reactive dye is remazol brilliant blue R (RBBR). This dye dissociates in water to produce negative ions. These negative ions are attracted to the positive polar side of water molecules, making RBBR molecules dissolve in textile effluents at a higher degree. Upon exposure to humans, animals, and aquatic plants for an adequate amount of time, RBBR can cause serious diseases since RBBR is carcinogenic, mutagenic, and toxic (Lellis et al., 2019).

Nowadays, the adsorption process by using activated carbon (AC) is the most economical-friendly and efficient method to treat a variety of contaminants from wastewater, namely synthetic dyes (Ahmad et al., 2021a, Ahmad et al., 2021b), heavy metals (Yusop et al., 2022a, Yusop et al., 2022b), pesticides (Aziz et al., 2021, Domergue et al., 2022), emerging contaminants (Quesada et al., 2022) and others. This versatility trait of AC is contributed by the high surface area and variety of surface functional groups occurring on the AC's surface. Commercial AC is usually derived from coal, lignite, and petroleum coke. However, the dependency on these materials as AC's precursor had shifted to agricultural wastes due to economically attractive and reduction in environmental pollution (Bazan-Wozniak et al., 2017). Examples of agricultural wastes that successfully converted to AC are kraft lignin (Brazil et al., 2022), acacia wood (Yusop et al., 2021b), orange peels (Ramutshatsha-Makhwedzha et al., 2022a), pomegranate peel (Azmier et al., 2021), durian peel (Yusop et al., 2021a), lemongrass peel (Ahmad et al., 2021a) and many others. The adsorption process is widely applied due to a relatively fast process and environmental compatibility (Rasoulzadeh et al., 2021, Mohammadi et al., 2016).

In this study, meranti wood was processed into become optimized AC (MWAC) to treat RBBR dye in wastewater. Process optimization in AC preparation is important to discover the conditions that can lead to the best possible response; thus, one can increase the efficiency of processes without increasing the cost at all. Response surface methodology (RSM) is a promising tool for optimization and is widely utilized by most studies (Giri et al., 2022, Motaghi et al., 2022, Rubio-Clemente et al., 2021). In a traditional optimization method, one variable is altered at one time whilst other variables are fixed at a constant value. The RSM can overcome the limitations of the traditional optimization method such as; (i) the neglect of interactive effects between variables, (ii) extensive numbers of experiments needed to determine the optimization levels, (iii) a laborious and time-consuming process, and (iv) the data obtained is less precise than expected (Mohammadi et al., 2017, Asgari et al., 2022). Besides optimization, this study also focussed on simulating the RBBR-MWAC adsorption process to determine the mass transfer coefficient, mass transfer rate, and adsorption rate by using Polymath software. These parameters enable researchers to understand better the movement of adsorbate molecules from the bulk phase to the solid phase. The classic kinetic models of pseudo-first-order (PFO) and pseudo-second-order (PSO) can provide the rate constant value for the overall adsorption process only. Another perk of this simulation study is that the value for adsorption surface area can be computed as well. This surface area value can be compared directly with the surface area obtained through a characterization test to validate the adequacy of the simulation model.

2. Materials and methods

2.1. Chemicals

Remazol brilliant blue R dye, RBBR ($C_{22}H_{16}N_2Na_2O_{11}S_3$) with a purity of 65 % was supplied by Sigma-Aldrich (M) Sdn. Bhd., Malaysia. KOH pellet with a purity of 85 % was supplied by Riedel-el Haen, Germany. Both carbon dioxide, CO_2 (99.80 %) and nitrogen, N_2 (99.99 %) were supplied by MOX Gases Berhad, Malaysia.

2.2. Preparation of MWAC

The precursor of meranti wood chip (5 – 10 mm) was collected from a furniture factory located at Sungai Petani, Kedah, Malaysia. Once obtained, the precursor was cleaned thoroughly with water and then, dehydrated in an oven for 72 h. The dried precursor was carbonized using a vertical furnace at 550 °C for 1 h, under N_2 gas. The produced char was impregnated with KOH at different impregnation ratios (IR), as calculated as follows:

$$IR = \frac{W_{KOH}}{W_{char}} \quad (1)$$

where both W_{KOH} and W_{char} are the weight of the KOH pellet and the weight of dried char, respectively. Then, a modified microwave oven (EMM2001W, Sweden) was used to heat the chemically activated char, with CO_2 gas purging through the microwave oven (150 cm^3/min) to provide physical activation. Produced MWAC was washed with 0.1 M HCl solution and later, wet MWAC was dried in an oven, before being kept in an air-tight container. The yield of MWAC was calculated using the following formula:

$$Yield(\%) = \frac{W_f}{W_i} \times 100\% \quad (2)$$

where W_f and W_i are the dried weight of AWAC and the dried weight of precursor, respectively. Characterization of MWAC was done in terms of pore characteristics, BET surface area, proximate analysis, elemental analysis, surface morphology, surface chemistry, zeta potential and XPS analysis using Micromeritics volumetric adsorption analyser (ASAP 2010), application of Brunauer-Emmet-Teller equation to the adsorption–desorption isotherm of N_2 at 77 K, simultaneous thermal analyzer (Perkin Elmer STA 6000, USA), elemental analyzer (Perkin Elmer Series II 2400, USA), scanning electron microscopy (SEM) (LEO SUPRA 55VP, Germany), Fourier trans-

forms infrared spectroscopy (FTIR) (Shidmazu Prestige 21, Japan), zeta potential analyzer (Zetasizer Nano Series DKSH), and X-ray photoelectron spectroscopy (XPS) (AXIS Ultra DLD, Kratos, UK), respectively.

2.3. Process variables and experimental design

This study aimed to produce MWAC with high RBBR dye removal and high yield. This was done by finding the MWAC's optimum preparation conditions by using the standard RSM design of Central Composite Design (CCD). The experimental data were analysed by a software known as Design Expert Software (STAT-EASE Inc. Minneapolis, USA) version 6.0.6. Three variables of radiation power, radiation time, and IR were selected and the ranges ($-\alpha$, -1, 0, $+1$, $+\alpha$) for these variables were (144 W, 264 W, 440 W, 616 W, 736 W), (2.64 min, 4.00 min, 6.00 min, 8.00 min, 9.36 min) and (0.00 g/g. 0.50 g/g, 1.25 g/g, 2.00 g/g, 2.51 g/g), respectively.

2.4. Batch adsorption studies

In batch adsorption studies, RBBR dye solutions with different initial concentrations (25, 50, 100, 200, 250, and 300 mg/L) were prepared. For each of these solutions, 200 mL was filled inside 250 mL of Erlenmeyer flasks. These flasks were transferred inside a shaker and 0.2 g of MWAC was added to each flask. The temperature and the agitation speed of the shaker were set to 30 °C and 120 rpm, respectively. The pH of RBBR solution was let to be original with no alteration during the batch adsorption studies. This process continues until adsorption equilibrium was reached. UV–vis spectrophotometry (Agilent Cary 60, USA) was used to determine the concentration of RBBR dye solution (λ_{max} = 592 nm). A small sample of RBBR solution was taken out using syringe that is equipped with a nylon filter (0.45 μm) to filter out any debris of MWAC. The amount of RBBR adsorbed by MWAC and RBBR dye removal percentage during equilibrium studies were calculated by using Eq. (3) and Eq. (4), respectively, as follows:

$$q_e = \frac{(C_o - C_e)V}{W} \tag{3}$$

$$\%Removal = \frac{C_o - C_e}{C_o} \times 100\% \tag{4}$$

where C_o, C_e, V, and W are the initial concentration of RBBR (mg/L), the concentration of RBBR at equilibrium (mg/L), the volume of solution (L), and the weight of MWAC used (g), respectively. Four isotherm models were used to verify the adsorption behaviour of RBBR onto MWAC. These isotherm models are Langmuir, Freundlich, Temkin, and Koble-Corrigan (KC), respectively:

Langmuir (Langmuir, 1918):

$$q_e = \frac{Q_m K_L C_e}{1 + K_L C_e} \tag{5}$$

Freundlich (Freundlich, 1906):

$$q_e = K_F C_e^{1/n_F} \tag{6}$$

Temkin (Tempkin and Pyzhev, 1940):

$$q_e = \frac{RT}{B} \ln(AC_e) \tag{7}$$

Koble-Corrigan (KC) (Koble and Corrigan, 1952):

$$q_e = \frac{a_{KC} C_e^{n_{KC}}}{1 + b_{KC} C_e^{n_{KC}}} \tag{8}$$

where Q_m is maximum adsorption capacity (mg/g); K_L is the constant of Langmuir that is related to adsorption capacity (mg/g); K_F ((mg/g)(L/mg)$^{1/n}$) and n_F (dimensionless) are constants of Freundlich; B and A are constants of Temkin whilst a_{KC}, b_{KC} and n_{KC} are constants for KC model. The more n_{KC} approaches 1, the more the KC model reduces to the Langmuir model. These non-linear equations were solved by using Microsoft Excel Solver version 2016. To verify the feasibility of the adsorption process, Langmuir dimensionless equilibrium constant, R_L can be calculated as follows:

$$R_L = \frac{1}{1 + K_L C_o} \tag{9}$$

2.5. Kinetic study

The kinetic study was conducted by measuring the concentration of six RBBR solutions (25–300 mg/L) at a pre-determined time interval between 0 and 180 min. The dosage of MWAC used was 0.20 g per 200 mL of RBBR solution. Other experiment conditions such as solution temperature and shaking speed of the water bath shaker were fixed at 30 °C and 80 rpm, respectively. The two most employed kinetic models of pseudo-first-order (PFO) and pseudo-second-order (PSO) were utilized in this study. Their non-linear equations are given as follows:

Pseudo-first order (PFO) (Lagergren, 1898):

$$q_t = q_e[1 - exp(-k_1 t)] \tag{10}$$

Pseudo-second order (PSO) (Ho and McKay, 1998):

$$q_t = \frac{k_2 q_e^2 t}{1 + k_2 q_e t} \tag{11}$$

where k_1 implies the rate constant for PFO (h^{-1}) and k_2 implies the rate constant for PSO (g/mg.h). These non-linear equations were solved by using Microsoft Excel Solver version 2016.

2.6. Simulation mass transfer study

A proposed mathematical model was used to represent the RBBR-MWAC adsorption system. Below is the material balance equation for RBBR uptakes by MWAC:

$$\frac{dC}{dt} = r_m + r_A \tag{12}$$

where C, r_m, and r_A denote the concentration of RBBR (mg/L), mass transfer rate (mg/s), and adsorption rate (mg/s), respectively. The mass transfer rate of RBBR from the bulk to the solid phase is as follows:

$$r_m = k_m a_m (C - C_e) \tag{13}$$

where k_m refers to the external mass transfer coefficient (mg.m/s), a_m represents the mass transfer area (m^2/g) whilst C and C_e denote the RBBR concentration at bulk phase and solid phase

(mg/L), respectively. By assuming a pseudo-first-order model, the connection between reaction rate (r_A) and RBBR concentration in an aqueous solution is given as follows:

$$r_A = -K_1(C - C_e) \tag{14}$$

where K_1 represents the adsorption rate constant (L/s). Combining Eq. (12), (13), and (14), the following equation is formed:

$$\frac{dC}{dt} = k_m a_m (C - C_i) - K_1(C - C_e) \tag{15}$$

Eq. (15) was integrated with initial conditions of X(t = 0) = X_0 and C(t = 0) = t_0. The resulting equation is shown as follows:

$$C = C_e - \exp(-t * (K_1 + a_m k_m)) * (C_e - C_o) \tag{16}$$

The parameters of mass transfer were determined by fitting the experimental results into Eq. (16), with the aid of Polymath® version 6.2 (CACHE Corporation, USA).

2.7. Thermodynamic study

Increasing solution temperature can alter the dynamic of the adsorption process significantly. Thermodynamic parameters of change of enthalpy, ΔH° (kJ/mol), and change of entropy, ΔS° (kJ/mol.K) computed using Van't Hoff equation as follows:

$$lnK_c = \frac{\Delta S^\circ}{R} - \frac{\Delta H^\circ}{RT} \tag{17}$$

where R, T, and K_c refer to gas constant (8.314 J/mol.K), solution temperature (K), and dimensionless constant of equilibrium. Lima et al. (2019) reported that the K_c value can be determined using the following formula:

$$K_c = \frac{1000 \frac{mg}{g} \times K_L \times molecularweightofadsorbate \times [adsorbate]^\circ}{\gamma} \tag{18}$$

where [adsorbate]° is the adsorbate's standard concentration at the standard state where this value can be considered as 1 mol/L, ϒ is the dimensionless constant of adsorbate's activity coefficient and K_L refers to the Langmuir constant of adsorption (L/mg). On the other hand, other thermodynamic parameters of Gibbs free energy, ΔG° (kJ/mol), and Arrhenius activation energy, E_a (kJ/mol) are determined from the equations as follows, respectively:

$$\Delta G^\circ = \Delta H^\circ - T\Delta S^\circ \tag{19}$$

$$lnk_2 = lnA - \frac{E_a}{RT} \tag{20}$$

where k_2 and A refer to PSO's rate constant and Arrhenius factor, respectively.

3. Results and discussions

3.1. Optimization studies

3.1.1. Regression models development

The complete experimental design matrix for MWAC's preparation is given in Table 1. For both responses studied, quadratic type of models was suggested by the software. These empirical models in the form of coded factors are given as follows:

RBBR uptakes (mg/g), Y_1:

$$Y_1 = 86.08 + 6.10X_1 + 3.06X_2 + 5.19X_3 - 7.03X_1^2 - 5.18X_2^2 - 3.98X_3^2 + 0.5187X_1X_2 + 0.5687X_1X_3 - 4.60X_2X_3 \tag{21}$$

MWAC's yield (%), Y_2:

$$Y_2 = 31.93 - 2.94X_1 - 2.47X_2 - 1.05X_3 - 3.26X_1^2 - 2.91X_2^2 - 4.83X_3^2 - 0.43X_1X_2 - 0.15X_1X_3 - 0.097X_2X_3 \tag{22}$$

The empirical models in the form of non-coded factors (actual equations) are given as follows:

RBBR uptakes (mg/g), Y_1:

$$\begin{aligned}\text{RBBR uptakes}\left(\frac{\text{mg}}{\text{g}}\right) = {} & -65.31015 \\ & + 0.220096\,\text{Radiation power} \\ & + 20.24329\,\text{Radiation time} \\ & + 41.13217\,\text{IR} \\ & + 0.001474\,\text{Radiation power} \\ & * \text{Radiation time} \\ & + 0.004309\,\text{Radiation power} \\ & * \text{IR} - 3.06917\,\text{Radiation time} \\ & * \text{IR} \\ & - 0.000227\,\text{Radiation power}^2 \\ & - 1.29379\,\text{Radiation time}^2 \\ & - 7.07770\text{IR}^2\end{aligned} \tag{23}$$

MWAC's yield (%), Y_2:

$$\begin{aligned}\text{MWAC}'\text{syield} = {} & -15.80832 \\ & + 0.084597\,\text{Radiation power} \\ & + 8.10206\,\text{Radiation time} \\ & + 20.94022\,\text{IR} \\ & - 0.001222\,\text{Radiation power} \\ & * \text{Radiation time} \\ & - 0.001136\,\text{Radiation power} * \text{IR} \\ & - 0.063333\,\text{Radiation time} * \text{IR} \\ & - 0.000105\,\text{Radiation power}^2 \\ & - 0.726723\,\text{Radiation time}^2 \\ & - 8.58666\,\text{IR}^2\end{aligned} \tag{24}$$

Fig. 1(a) and (b) present the plots of predicted versus actual for RBBR uptakes response and MWAC's yield response, respectively. The predicted values for RBBR uptakes response were obtained from Eq. (21) and (23) whilst the predicted values for MWAC's yield were obtained from Eq. (22) and (24). The actual values for both responses were obtained from the experiment. The adequacy of Eq. (21) and (22) were verified in terms of R^2, adj-R^2, standard deviation (SD), and adequate

Table 1 Complete experimental design matrix for MWAC's preparation.

Run	MWAC's preparation variables			Responses	
	Radiation power, X_1 (watt)	Radiation time, X_2 (min)	IR, X_3	RBBR removal, Y_1 (%)	MWAC's yield, Y_2 (%)
1	440 (0)	6.00 (0)	2.51 (+α)	82.55	14.92
2	264 (-1)	4.00 (-1)	2.00 (+1)	73.15	25.04
3	440 (0)	6.00 (0)	1.25 (0)	88.11	33.19
4	736 (+α)	6.00 (0)	1.25 (0)	79.34	15.94
5	440 (0)	2.64 (-α)	1.25 (0)	65.85	27.63
6	264 (-1)	8.00 (+1)	0.50 (-1)	67.35	22.87
7	440 (0)	6.00 (0)	1.25 (0)	87.13	32.87
8	264 (-1)	4.00 (-1)	0.50 (-1)	51.89	26.87
9	440 (0)	6.00 (0)	1.25 (0)	84.11	30.13
10	616 (+1)	4.00 (-1)	0.50 (-1)	61.44	22.12
11	440 (0)	9.36 (+α)	1.25 (0)	77.55	17.85
12	440 (0)	6.00 (0)	1.25 (0)	86.86	32.32
13	616 (+1)	8.00 (+1)	2.00 (+1)	80.56	15.05
14	440 (0)	6.00 (0)	0.00 (0)	67.86	19.9
15	616 (+1)	4.00 (-1)	2.00 (+1)	81.44	21.15
16	264 (-1)	8.00 (+1)	2.00 (+1)	66.66	22.12
17	440 (0)	6.00 (0)	1.25 (0)	84.75	31.45
18	440 (0)	6.00 (0)	1.25 (0)	85.44	31.99
19	616 (+1)	8.00 (+1)	0.50 (-1)	75.44	17.86
20	144 (-α)	6.00 (0)	1.25 (0)	53.51	27.52

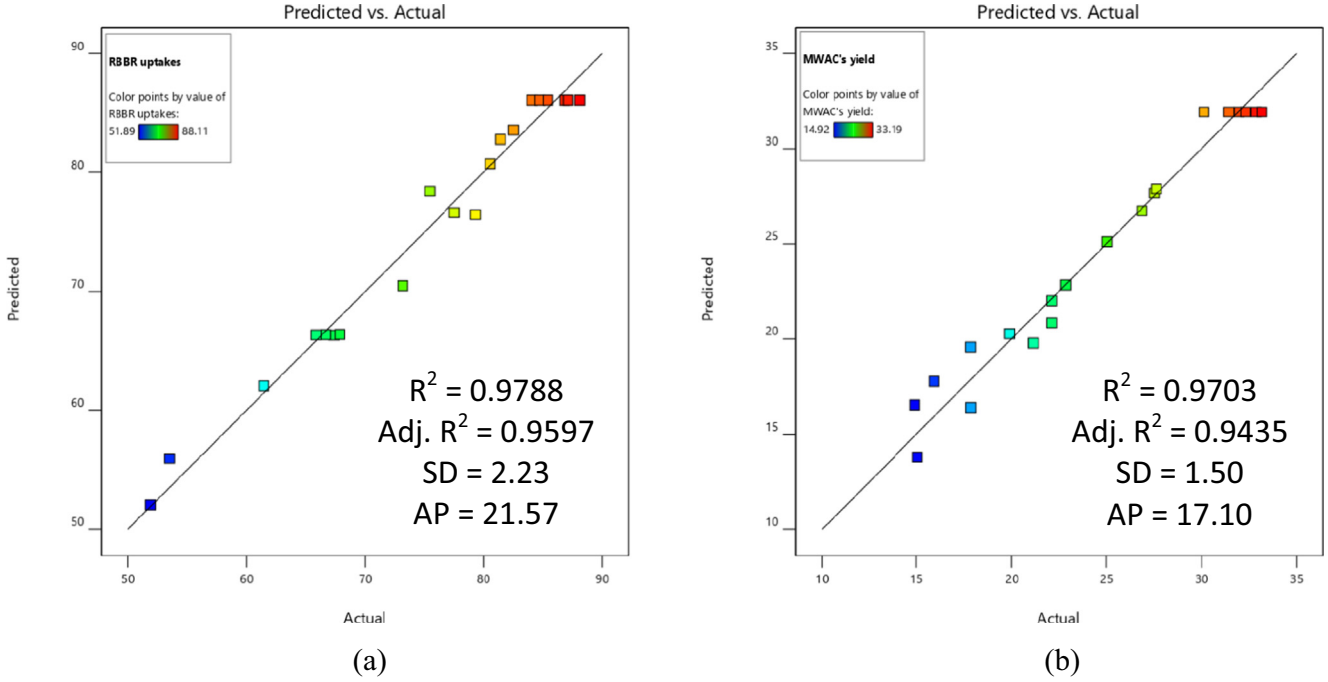

Fig. 1 Plots of predicted versus actual for (a) RBBR uptakes and (b) MWAC's yield.

precision (AP). Both of these models were excellent due to the high R^2 and adj-R^2 obtained of (0.9788 and 0.9597) and (0.9703 and 0.9435), respectively. Adj-R^2 values were important since insignificant terms were omitted in its calculation. Both equations produced small SD of 2.23 and 1.50, respectively, therefore signifying low deviation between experimental and calculated data. AP values were determined to be 21.57 and 17.10 for both equations, respectively. Since these values were above 4, therefore the developed models were adequate to navigate the design space.

3.1.2. Analysis of variance (ANOVA)

The adequacy of the developed models can be further verified through analysis of variance (ANOVA). The result of

Table 2 ANOVA results for responses studied.

Source	Response 1, Y_1: RBBR removal by MWAC					Response 2, Y_2: MWAC's yield				
	Sum of Squares	DF	Mean Square	F Value	Prob > F	Sum of Squares	DF	Mean Square	F Value	Prob > F
Model	2297.72	9	255.30	51.23	< 0.0001	734.12	9	81.57	36.26	< 0.0001
X_1	507.73	1	507.73	101.89	< 0.0001	118.30	1	118.30	52.59	< 0.0001
X_2	127.72	1	127.72	25.63	0.0005	83.28	1	83.28	37.02	0.0001
X_3	366.18	1	366.18	73.48	< 0.0001	15.13	1	15.13	6.73	0.0268
X_1X_2	2.15	1	2.15	0.4320	0.5258	1.48	1	1.48	0.6576	0.4363
X_1X_3	2.59	1	2.59	0.5193	0.4876	0.1800	1	0.1800	0.0800	0.7830
X_2X_3	169.56	1	169.56	34.02	0.0002	0.0722	1	0.0722	0.0321	0.8614
X_1^2	712.36	1	712.36	142.95	< 0.0001	153.10	1	153.10	68.06	< 0.0001
X_2^2	384.83	1	384.83	77.22	< 0.0001	121.42	1	121.42	53.98	< 0.0001
X_3^2	224.85	1	224.85	45.12	< 0.0001	330.95	1	330.95	147.12	< 0.0001

ANOVA for both responses are shown in Table 2. Since the Prob > F value for the models of Y_1 and Y_2 were < 0.0001, therefore both of these models were significant. The significant terms for Y_1 were X_1, X_2, X_3, X_2X_3, X_1^2, X_2^2 and X_3^2 whilst significant terms for Y_2 were X_1, X_2, X_3, X_1^2, X_2^2 and X_3^2. By judging F-value, the response of Y_1 was significantly affected by radiation power and IR whereas the response of Y_2 was greatly influenced by radiation power and radiation time.

3.1.3. Three-dimensional (3D) response surface of MWAC

Each of the variables studied affects the responses of Y_1 and Y_2 differently. These effects can be better understood by examining the three-dimensional (3D) response surface. Fig. 2 shows the 3D surface plot for (a) RBBR uptakes, Y_1 (effects of radiation power and IR), and (b) MWAC's yield, Y_2 (effects of radiation power and radiation time). Based on Fig. 2(a), when radiation power and IR were at their lowest values of 264 W and 0.50 g/g, respectively, the lowest RBBR dye removal by MWAC occurred. As both of these variables increased, RBBR dye removal increased accordingly. This can be explained by the fact that at higher radiation power, more volatile matter and tar compounds are successfully removed due to the enhanced cracking reaction, thus creating more pores and increasing adsorption capacity (Wan Mahari et al., 2016). According to Rashidi and Yusup (2017), higher IR can help create more pores by providing an extra amount of K^+ ions to penetrate the char, thus increasing the adsorption capacity. However, at an extremely high level of radiation power and IR, a small dropped in RBBR dye removal was noticed. At an extremely high level of radiation power, excess energy is causing a certain amount of carbon to be burned, thus reducing existing pores and adsorption capacity. Likewise, by increasing the IR level beyond the optimum level, excess K^+ ions are trapped inside the existing pores, thus reducing adsorption capacity. Based on Fig. 2(b), radiation power and radiation time were found to have a negative effect on MWAC's yield. In fact, the highest MWAC's yield was obtained when both of these variables were at the lowest level of 264 W and 8.00 min, respectively. An increase in radiation power leads to a higher degree of volatilization process to

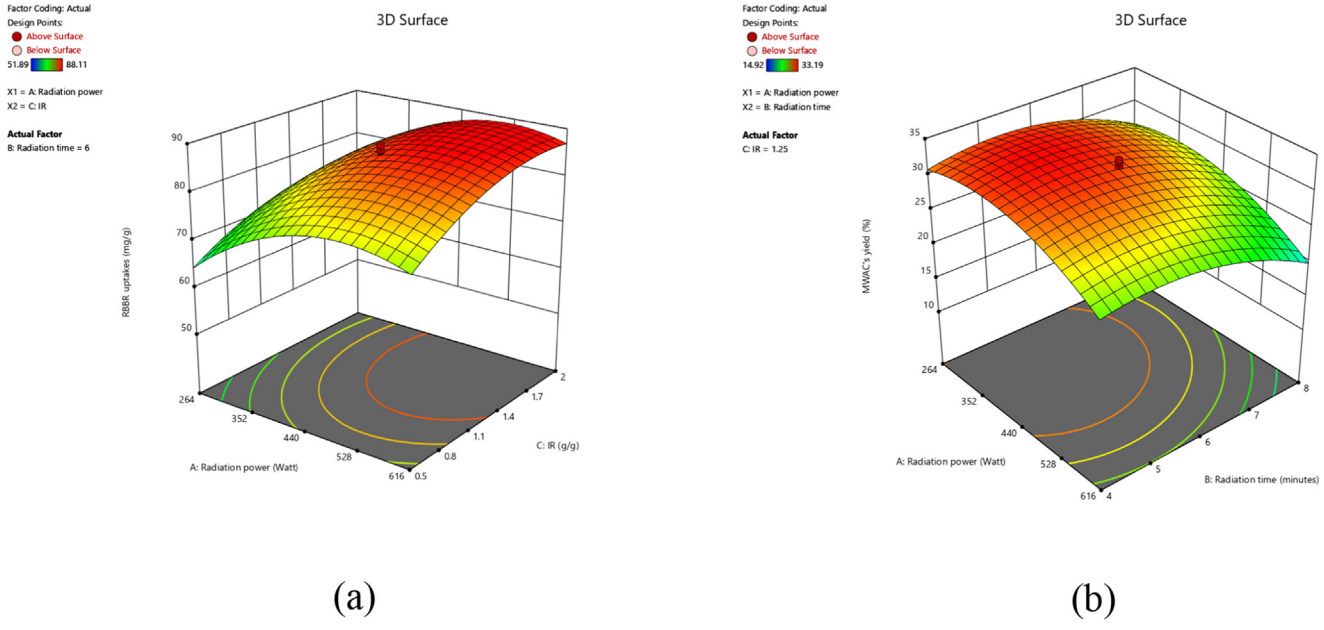

Fig. 2 3D response surface plots for (a) RBBR dye removal and (b) MWAC's yield.

occur, thus reducing more of MWAC's weight. Furthermore, by increasing radiation time, the aggressive volatilization process would occur for a longer period of time, therefore reducing MWAC's weight even further. A similar finding was reported by Ghani et al. (2017) where the yield of the sample decreased significantly after being exposed to microwave heating beyond the optimum range of radiation time.

3.1.4. Optimization of MWAC's preparation variables

Table 3 presents the optimization data for the variables and responses studied. The optimization process was executed by setting the responses studied as "maximum" and the variables studied as "in range". As the result, the optimum values generated by the software were found to be 441 W, 5.77 min, and 1.35 g/g for radiation power, radiation time and IR, respectively which produced 86.39 mg/g and 31.94 % of RBBR uptakes and MWAC's yield, respectively. The models were validated to be excellent in predicting the responses due to the small error percentage obtained for RBBR dye removal (2.14 %) and MWAC's yield (0.85 %). The desirability for this solution was relatively high of 0.942.

3.2. Characterization of MWAC

The elemental and proximate analyses are given in Table 4. The precursor was found to be composed of 33.20 % of C element, 7.52 % of H element, 0.21 % of S element, and 59.07 % of N + O elements whilst MWAC was revealed to be comprised of 81.94 % of C element, 1.59 % of H element, 0.11 % of S element, and 16.36 % of N + O elements. The proximate analysis revealed that after carbonization and activation processes took place, moisture and volatile matter decreased significantly from 10.28 % and 59.22 % in the precursor to 4.74 % and 10.19 % in MWAC, respectively. These components evaporated and left the sample, causing the fixed carbon to rise from 28.15 % in the precursor to 83.16 % in MWAC. The selection of meranti wood as the precursor was the right decision in the first place due to the relatively high fixed carbon percentage that it posed. Precursors with a high percentage of fixed carbon can produce AC with good performance since the fixed carbon made up the carbon matrix structure in AC. In comparison, other biomasses pose lower fixed carbon percentages such as pine wood of 26.50 % (Ahmed et al., 2019), acacia wood of 24.75 % (Yusop et al., 2021b), and Jatoba barks of 23.60 % (Spessato et al., 2019). Besides that, another good trait of meranti wood is the low ash percentage of 2.35 %. Ash is not desired in AC since ash does not have any pores, thus ash does not contribute to the adsorption process.

Physicochemical activation employed succeeded in increasing the BET surface area and mesopores surface area from 453.25 m^2/g and 278.11 m^2/g in char to 1257.22 m^2/g and 825.58 m^2/g in MWAC, respectively. During chemical activation, K^+ penetrates deep into the skeleton of the char, resulting development of a new pores network while during physical activation, CO_2 gas molecules bombarded the surface of the sample, making the existing pores to be bigger in size besides assisting new pores to be developed. The pores in MWAC lie in the mesopores region due to an average pore diameter of 2.48 nm and a total pore volume of 0.5870 cm^3/g. The surface morphology of the precursor and MWAC was studied by inspecting their SEM images, as shown in Fig. 3. The surface of the precursor was found to contain no pores whereas the surface of MWAC was spotted to be packed with pores distributed all over the places. Originally, these pores are the home for the moisture content, volatile matter, and tar compound that were successfully removed by effective carbonization and physicochemical activation.

The functional groups existed on the surface of precursor and MWAC was identified by studying their FTIR spectrum, as given in Fig. 4. Peaks that can be seen on both spectrum of precursor and MWAC were alkyne C—H bend (632 and 575 cm^{-1}), methylene $(CH_2)n$ (750 and 612 cm^{-1}), cyclohexane ring vibrations (1013 and 832 cm^{-1}), C=C–C aromatic ring stretch (1512 and 1191 cm^{-1}), alkyl carbonate (1747 and 1543 cm^{-1}), aryl carbonate (1791 and 1609 cm^{-1}), aliphatic primary amine, NH stretch (3390 and 3310 cm^{-1}) and non-bonded hydroxy group, OH stretch (3645 and 3530 cm^{-1}), respectively. Unlike them, some functional groups were badly affected by physicochemical activation and microwave heating, thus they only existed on precursor, such as nitrate ions

Table 3 Optimization data for variables and responses studied.

Variables			Responses						Model desirability
Radiation power, X_1 (W)	Radiation time, X_2 (min)	IR, X_3 (g/g)	RBBR uptakes, Y_1 (mg/g)			MWAC's yield, Y_2 (%)			
			Actual	Predicted	Error (%)	Actual	Predicted	Error	
441	5.77	1.35	88.28	86.39	2.14	32.21	31.94	0.85	0.942

Table 4 Proximate and elemental analyses of the samples.

	Proximate analysis (%)				Elemental analysis (%)			
	Moisture	Volatile matter	Fixed carbon	Ash	C	H	S	(N + O)
Precursor	10.28	59.22	28.15	2.35	33.20	7.52	0.21	59.07
MWAC	4.74	10.19	83.16	1.91	81.94	1.59	0.11	16.36

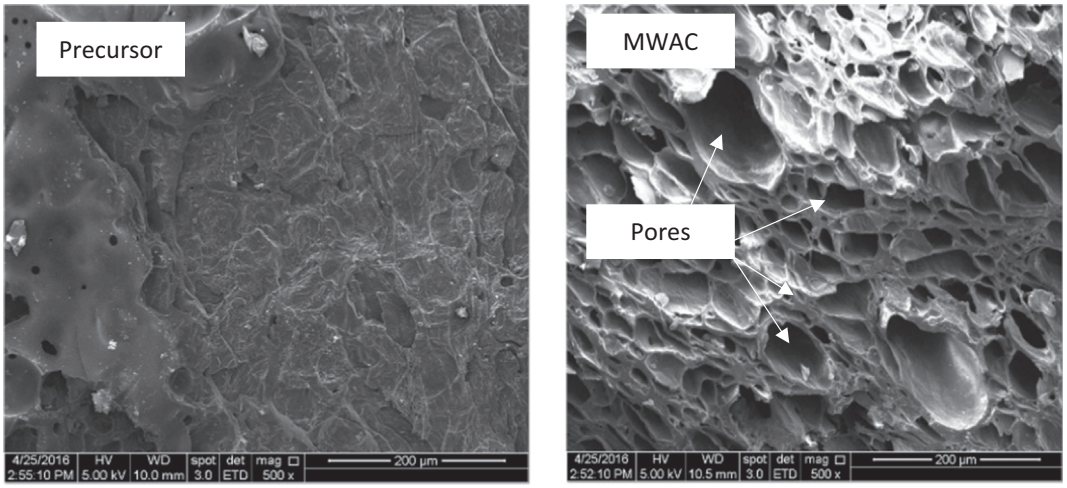

Fig. 3 SEM images of precursor and MWAC.

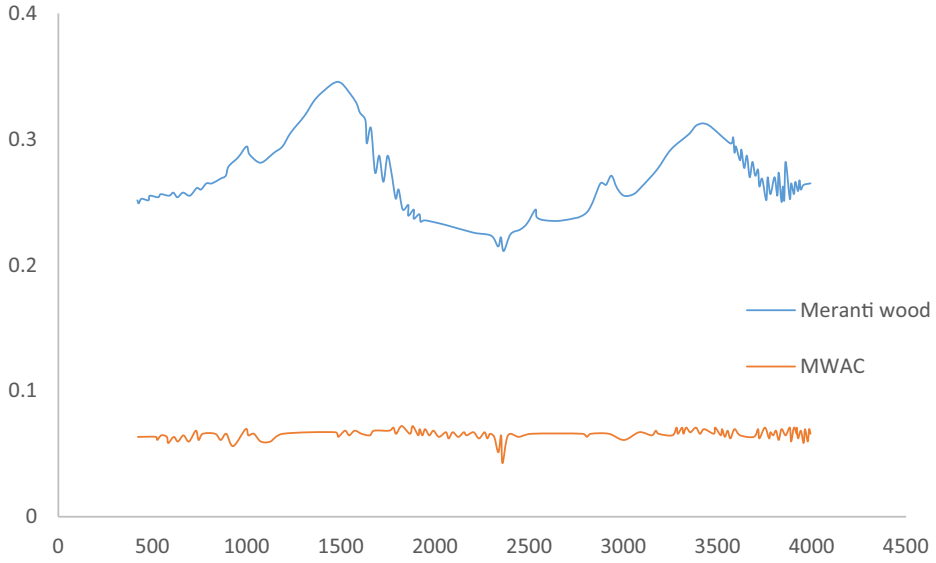

Fig. 4 FTIR spectrum for (a) precursor and (b) MWAC.

(815 cm^{-1}), alkenyl C═C stretch (1629 cm^{-1}), carboxylic acid (1703 cm^{-1}), methylene C—H asymmetric (2935 cm^{-1}). New peaks were formed on MWAC's surface namely C≡C terminal alkyne (1969 cm^{-1}), C≡C medial alkyne (2071 cm^{-1}), methoxy, C—H stretch (CH_3-O) (2386 cm-1), vinyl C—H stretch (2511 cm-1), alkyne C—H stretch (3083 and 3149 cm^{-1}), phenols, O—H stretch (3318 cm^{-1}) and tertiary alcohol, O—H stretch (3400 cm^{-1}). Fig. 5 shows the possible interactions occurred between functional groups and RBBR molecules. Functional groups of methylene and alkyne formed hydrogen bonds with RBBR molecules, alkyl carbonate, terminal alkyne and methoxy interacted with RBBR molecules via dipole–dipole force whilst primary amine and alcohol formed ion dipole force with RBBR molecules.

Fig. 6 presents the XPS spectra for MWAC. Based on these spectra, it was found that MWAC posed atomic concentration of C (75.91 %), O (18.01 %), N (1.25 %) and Si (4.83 %). This result was consistent with the elemental analysis where C element posed the highest elemental percentage, followed by the combination of O and N elements. Small atomic composition of Si in MWAC came from the ash component which is consistent with the result of proximate analysis.

3.3. Adsorption equilibrium

3.3.1. Effect of contact time and initial MB dye concentration

The plots of adsorption uptakes versus time and percentage removal versus time at different RBBR initial concentration are given in Fig. 7(a) and (b), respectively. When RBBR initial concentration increased from 25 to 300 mg/L, adsorption uptakes of RBBR increased from 22.94 to 210.15 mg/g. At higher concentration, larger mass transfer driving force occurred to enable RBBR molecules to triumph mass transfer resistance (Yusop et al., 2021b). On contrary, RBBR percentage removal dropped from 91.77 to 70.05 % when RBBR concentration increased from 25 to 300 mg/L. At lower initial

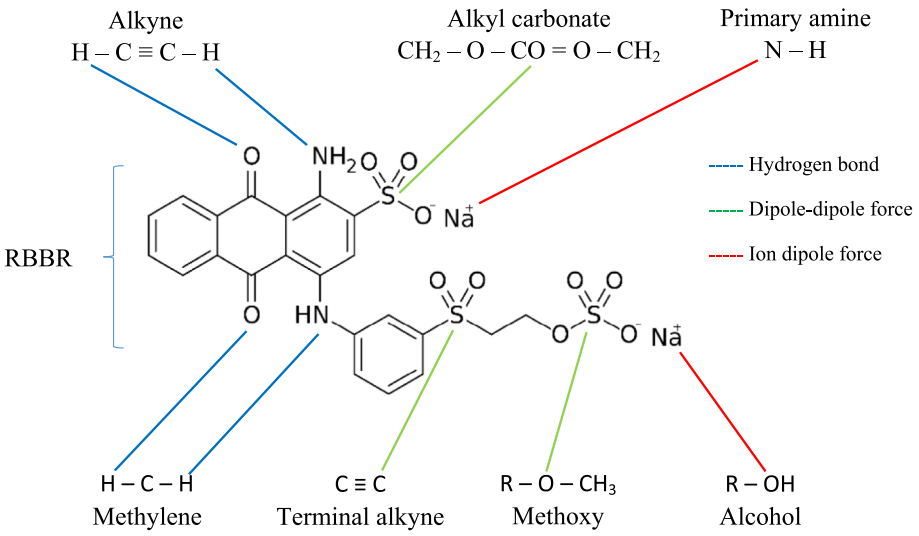

Fig. 5 Possible interactions between RBBR molecules and surface functional groups.

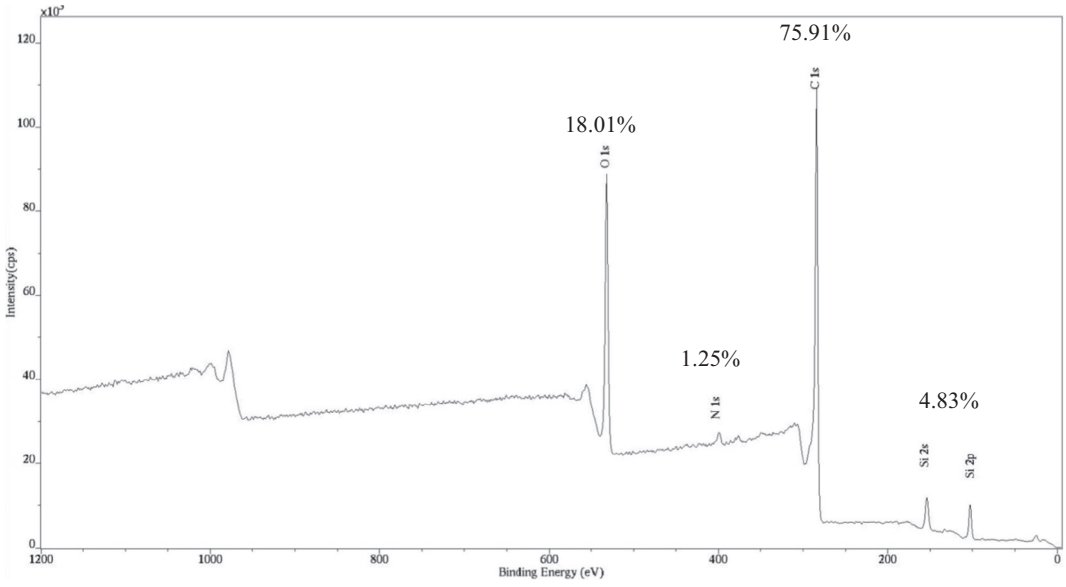

Fig. 6 XPS spectra for MWAC.

concentration, a smaller number of RBBR molecules available, thus less competition occurred among them to be adsorbed. Less adsorption competition at lower initial concentration also causing the adsorption system at 25 and 50 mg/L to achieve equilibrium state faster at 4 to 5 h. In contrast, higher initial concentration of 100 to 300 mg/L required 7 h to achieve the same state.

3.3.2. Effect of solution temperature and pH

By raising the solution temperature from 30 to 50 °C, a reduction in RBBR adsorption uptakes occurred from 82.33 to 76.25 mg/g. At higher solution temperatures, the performance of MWAC in adsorbing RBBR becomes poorer due to the increased solubility of RBBR dye molecules in the solution. In addition, adsorbate molecules posed higher kinetic energy at higher solution temperatures, thus making it easier for them to flee from the solid phase to the bulk phase (Abbaszadeh et al., 2016). Furthermore, Doumic et al. (2015) stated that electrostatic interaction between anionic RBBR dye and polar functional groups that existed on MWAC's surface becomes weaker at higher solution temperatures, thus promoting the desorption process. The plots of RBBR uptakes by MWAC under different solution temperature and solution pH is given in Fig. 8(a) and (b), respectively whilst the zeta potential value for MWAC at pH 2 and 12 are given in Table 5. It was revealed that MWAC performed the best and the worst in removing RBBR dye at pH 2 (87.42 mg/g) and pH 12 (64.21 mg/g), respectively. At pH 12 (alkaline condition), a large amount of OH^- ions existed in the solution and inducing the MWAC's surface to be negatively charged. As a consequence, an electrostatic repulsion occurs between anionic RBBR dye molecules and MWAC's surface which led to the drop in MWAC's adsorption performance. This was supported by the zeta potential value of the −19.60 mV for

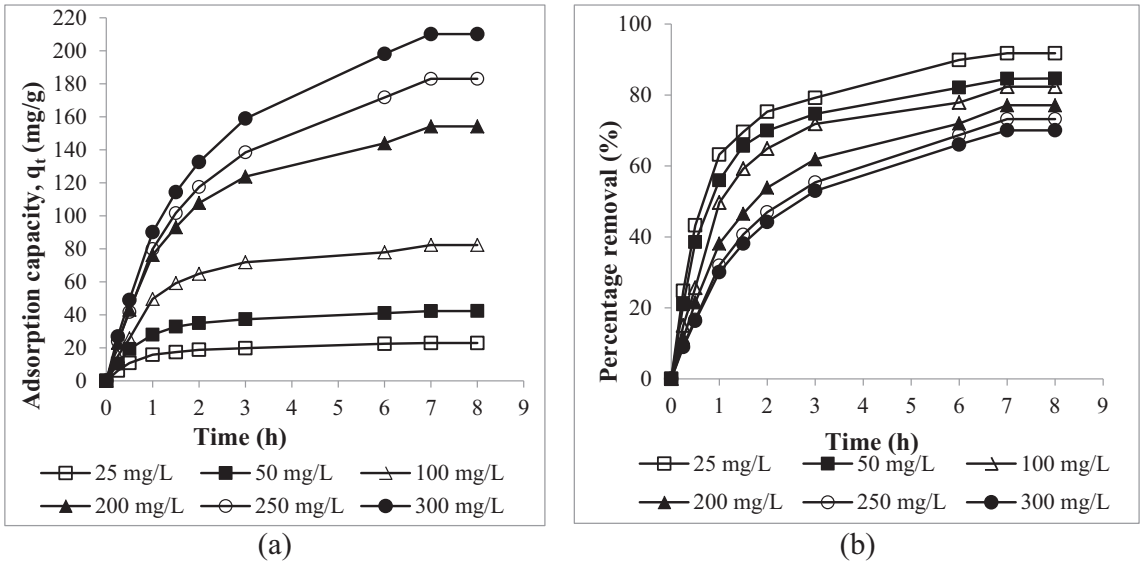

Fig. 7 The plots of (a) adsorption uptakes and (b) percentage removal of RBBR by MWAC versus time for different initial concentration.

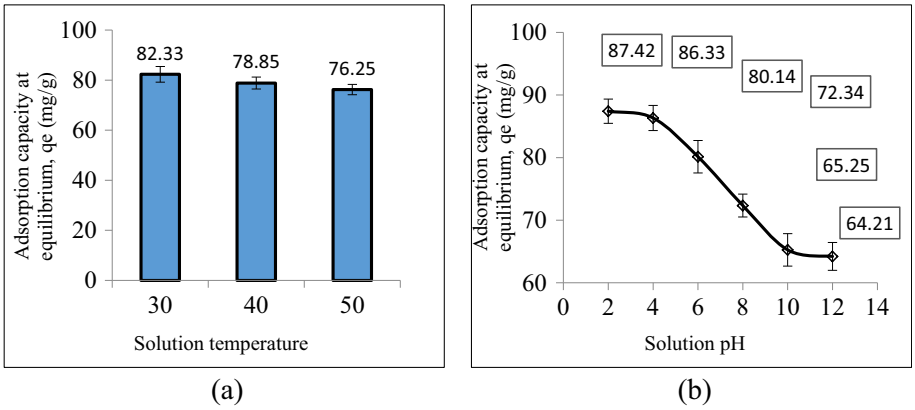

Fig. 8 The plots of RBBR uptakes by MWAC under different (a) solution temperature and (b) solution pH.

MWAC at pH12 (MWAC-pH12). The negative sign of zeta potential value signifies that the surface of MWAC-pH12 was filled with negatively charged surface functional groups. At pH 2 (acidic condition), excess H^+ ions are present in the solution and inducing the surface of MWAC to be less negatively charged, thus reducing the electrostatic repulsion between anionic RBBR dye molecules and MWAC's surface. This was supported by the zeta potential value of −2.08 mV for MWAC at pH2 (MWAC-pH2). Although the zeta potential value for MWAC-pH2 is still negative, its magnitude had dropped significantly as compared to MWAC-pH12. Therefore, it proved the effect of H^+ in reducing the negative charge on MWAC's surface.

Table 5 Zeta potential value for MWAC at pH2 and pH12.

	MWAC-pH2	MWAC-pH12
Zeta potential (mV)	−2.08	−19.60
Conductivity (mS/cm)	37.1	25.30

3.4. Adsorption isotherm

The isotherm plots are provided in Fig. 9 and all the parameters obtained from the isotherm models are presented in Table 6. Three models of Langmuir, Freundlich, and Koble-Corrigan (KC) produced low RMSE values of 4.41, 5.59, and 3.40, respectively. But between these three models, the Freundlich model was able to predict the experimental data the best, thus yielding the lowest error percentage of 4.86 %. Therefore, this adsorption process obeyed the Freundlich model, signifying multilayer coverage of RBBR onto MWAC's surface. More than one RBBR molecule can be absorbed by MWAC, and the strength of each bond is not homogenous. Besides that, the more RBBR molecules were absorbed in one active site, the lower the probability of another molecule binding to the exact active site because a higher energy is needed (Ammendola et al., 2017). The parameter from Freundlich isotherm, n_F was found to be 1.69 and since this value is between 1 and 10, it signifies that the adsorption process was favourable as well. Despite of low RMSE and average error

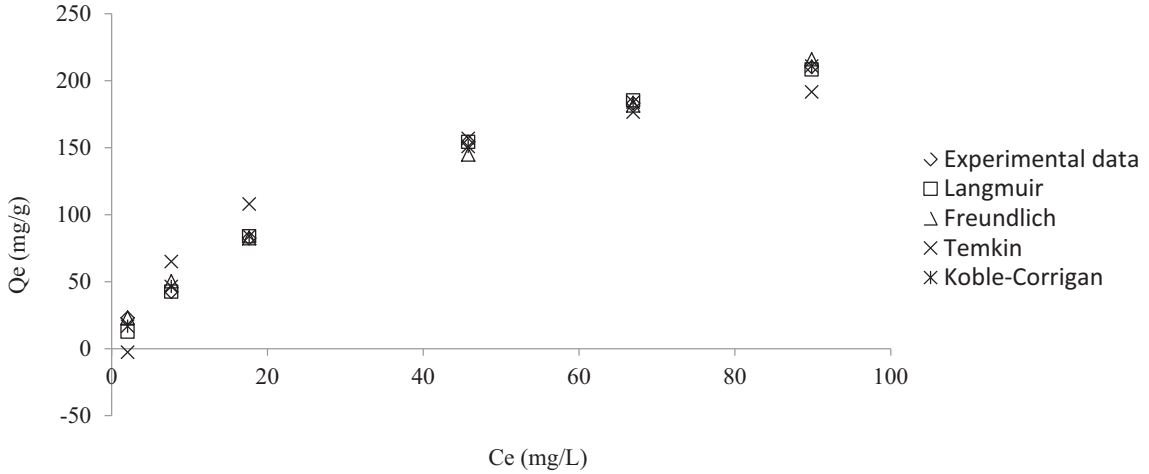

Fig. 9 Non-linear isotherm plots for RBBR-MWAC adsorption system at 30 °C.

Table 6 Isotherm parameters for RBBR-MWAC adsorption system at 30 °C.

Langmuir		Freundlich		Temkin		KC	
Q_m (mg/g)	327.33	n_F	1.69	B (L/mg)	51.48	A_{KC}	9.57
K_L (L/mg)	0.019	K_F (mg/g)(L/mg)$^{1/n}$	15.04	A (L/mg)	0.46	B_{KC}	0.02
						n_{KC}	0.83
RMSE	4.41	RMSE	5.59	RMSE	19.23	RMSE	3.40
Error (%)	8.21	Error (%)	4.86	Error (%)	35.10	Error (%)	6.88

produced by Koble-Corrigan, this model is invalid to describe the adsorption process study since the n_{KC} value was found to be 0.83 which is < 1 (Koble and Corrigan, 1952, Mozaffari Majd et al., 2022). Langmuir monolayer adsorption capacity, Q_m obtained was 327.33 mg/g and this value was relatively high as compared to RBBR removal by sewage sludge biochar of 126.59 mg/g (Raj et al., 2021), RBBR removal by bone char of 20.60 mg/g (Bedin et al., 2017) and RBBR removal by acacia sawdust based AC of 263.16 mg/g (Yusop et al., 2017). A further comparison between MWAC's adsorption performance with other biomass-based AC is summarized in Table 7. The equilibrium constant, R_L was found to be 0.15. Since this value is between 0 and 1, therefore the adsorption process studied was found to be favourable (Chen et al., 2021). In literature, besides dyes, few studies reported the adsorption of heavy metals onto meranti-based adsorbents. For instance, the meranti-based adsorbent was found to remove Cd(II), Cu(II), Cr(II), Ni(II), and Pb(II) with adsorption capacities of 175.43, 32.05, 37.88, 35.97, and 34.25 mg/g, respectively (Rafatullah et al., 2009, Rafatullah et al., 2012). Another study performed by Ahmad et al. (2009) found that meranti-based adsorbent can adsorb 37.17 mg/g of Cu(II) and 37.04 mg/g of Pb(II).

3.5. Adsorption kinetic

Fig. 10(a) and (b) present the non-linear kinetic plots for the PFO model and PSO model, respectively, whilst Table 8 shows the kinetic data. It was found that the adsorption of RBBR

Table 7 Adsorption performance of MWAC and other biomass-based AC.

AC's precursor	Adsorbate (dye)	Maximum adsorption capacity (mg/g)	References
Meranti wood	RBBR	327.33	This study
Walnut shell	Methylene blue	307.40	(Vakili et al., 2023)
Durian peel	Malachite green	231.17	(Yusop et al., 2021a)
Date palm frond	Eosin yellow	217.00	(Jabbar et al., 2022)
Rice husk	Crystal violet	235.70	(Goswami and Kumar Dey, 2022)
Mangosteen peel	Methylene blue	163.60	(Jawad et al., 2022)
Peltophorum pterocarpum leaf	Acid blue 9	151.00	(Subba Reddy et al., 2023)
	Rhodamine blue	170.10	
	Safranine O	221.81	
	Malachite green	272.66	
Orange and lemon peel	Methyl orange	33.00	(Ramutshatsha-Makhwedzha et al., 2022b)
	Methylene blue	38.00	

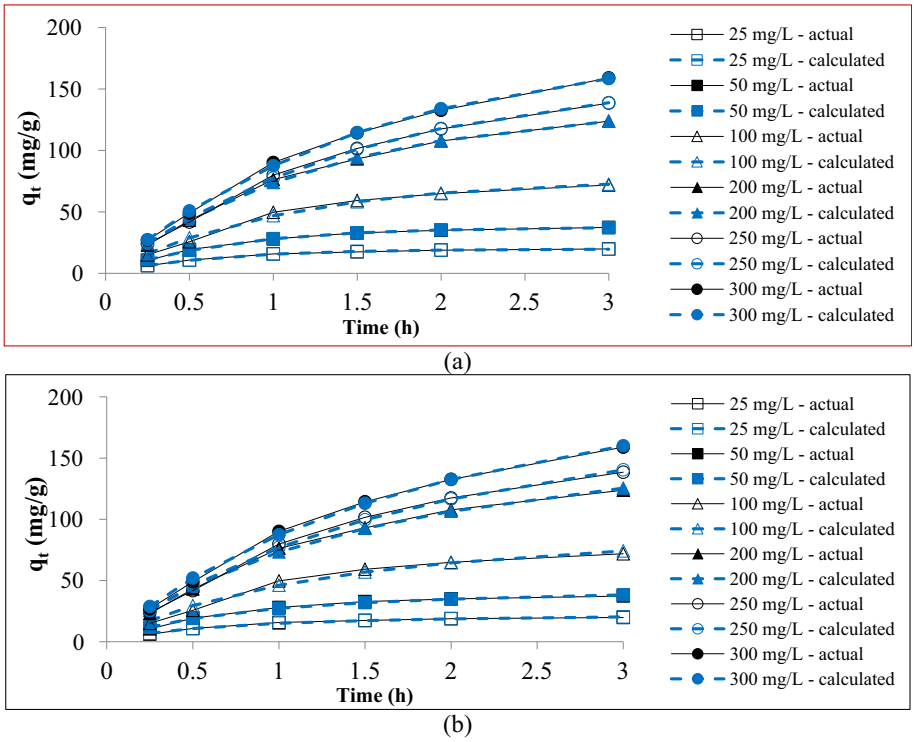

Fig. 10 Non-linear kinetic plots of (a) PFO and (b) PSO for RBBR-MWAC adsorption system at 30 °C.

Table 8 Kinetic parameters for RBBR-MWAC adsorption system at 30 °C.

Initial concentration (mg/L)	q_e, exp (mg/g)	PFO			PSO		
		k_1 (h^{-1})	q_e, cal (mg/g)	Error (%)	k_2 (g/mg.h)	q_e, cal (mg/g)	Error (%)
25	19.81	1.55	19.78	0.14	0.0635	24.65	24.48
50	37.34	1.37	37.71	0.98	0.0276	47.96	28.45
100	71.86	0.93	77.29	7.56	0.0072	106.55	48.27
200	123.76	0.77	137.09	10.77	0.0031	194.40	57.08
250	138.48	0.65	161.73	16.79	0.0020	237.93	71.82
300	158.94	0.64	186.07	17.07	0.0017	273.72	72.21
Average				***8.89***			***50.39***

dye onto MWAC was best represented by PFO kinetic model due to a lower average error percentage of 8.89 %. Therefore, PFO kinetic model can predict the adsorption uptakes, q_t with higher accuracy as can be seen in Fig. 10(a). Alberti et al. (2012) stated that four steps occur in the adsorption process. The first step is the transport of adsorbate molecules to the adsorbent. The second step is the diffusion of the adsorbate molecules through the film layer surrounding the adsorbent. The third step involves intraparticle diffusion and the last step involves physisorption or chemisorption. According to McGinley et al. (2022), PFO signifies that the rate limiting step in the adsorption process is caused by the first step, which is the transport of adsorbate to the adsorbent. The value of k_1 was found to decrease from 1.55 to 0.64 h^{-1} when RBBR initial concentration increased from 25 to 300 mg/L. At a higher adsorbate concentration, the ratio of adsorbate molecules to the available active sites on the adsorbent is high. Therefore, the adsorbate molecules compete to be adsorbed by the adsorbent at an intense level. As the consequence, the overall rate constant becomes lower at higher adsorbate concentrations and vice versa.

3.6. Adsorption mass transfer simulation

Polymath version 6.2 (CACHE Corpn., USA) was used to model the adsorption data to find the mass transfer and rate parameters. Fig. 11 shows the plot of mass transfer simulation. Table 9 summarized the mass transfer parameters obtained for this adsorption process. As RBBR concentration increased from 25 to 300 mg/L, mass transfer rate, r_m, and rate constant, K_1 increased from 112.20 to 10007.50 s^{-1} and from 3.96 to 4.34 h^{-1}, respectively. At higher RBBR initial concentration, a higher concentration slope between RBBR at bulk and solid phase occurred, thus causing higher mass transfer driving force

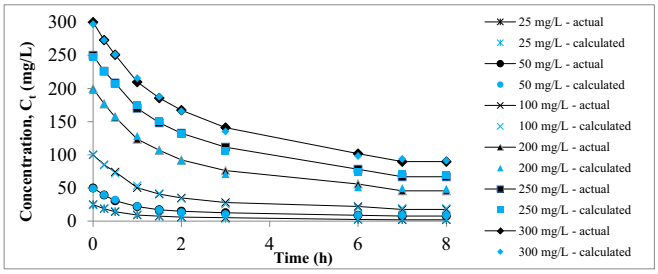

Fig. 11 The plot of mass transfer simulation.

Table 9 Summary of mass transfer parameters.

RBBR concentration (mg/L)	Mass transfer coefficient, K_m (mg.m/s)	Mass transfer rate, r_m (mg/s)	Rate constant, K_1 (L/s)	Adsorption surface area, a_m (m^2/g)	R^2	RMSD
25	0.006350	112.20	3.9591	798.30	0.9863	0.2719
50	0.006378	209.98	4.0326	801.80	0.9928	0.3708
100	0.006333	405.92	4.1833	796.21	0.9952	0.6133
200	0.006243	741.01	4.2813	784.90	0.9963	1.0100
250	0.006203	876.50	4.3305	779.87	0.9972	1.0554
300	0.006198	1007.50	4.3373	779.19	0.9979	1.0678
			Average:	**790.04**	**0.9943**	**0.7315**

to form. As the result, higher r_m and K_1 were obtained at higher RBBR concentrations. This model predicted the average adsorption surface area, a_m to be 790.04 m^2/g. This value was accurately close to the actual mesopores surface area of 825.58 m^2/g (error = 4.50 %), signifying the accuracy of the model developed. Further adequacy of this model was verified based on high R^2 values (0.9863 to 0.9979) and low RMSD (0.2719 to 1.0678) obtained.

3.7. Adsorption thermodynamic

The effect of temperature on the adsorption behaviour can be evaluated by determining the thermodynamic parameters which include enthalpy change (ΔH°), entropy change (ΔS°), Gibbs free energy (ΔG°), and Arrhenius activation energy, E_a. The enthalpy change, ΔH° was determined to be −4.06 kJ/-mol. A negative sign for this value signified the exothermic nature of the adsorption process where RBBR uptakes were higher at lower solution temperatures (Singh and Kuma, 2016). The value for entropy change, ΔS° was −0.06 kJ/mol. K, and the negative sign of this parameter indicates a reduction in randomness at the solid–liquid interface (Tharaneedhar et al., 2017). Arrhenius activation energy, E_a was calculated to be 16.03 kJ/mol and since this value lies between 5 and 40 kJ/mol, therefore the adsorption process was confirmed to be controlled by physisorption. The Gibbs free energy, ΔG° was found to be −22.69 kJ/mol. Due to the negative sign for this parameter, it can be concluded that the adsorption process was feasible and spontaneous in nature.

4. Conclusions

Meranti wood chip was successfully converted into MWAC to adsorb RBBR dye with a relatively high Q_m of 327.33 mg/g. MWAC was found to pose a high BET surface area and mesopores surface area of 1257.22 m^2/g and 825.58 m^2/g, respectively. With the aid of RSM, optimum preparation conditions were determined to be 441 W, 5.76 min, and 1.35 g/g for radiation power, radiation time, and IR, respectively which are responsible for producing MWAC with RBBR dye removal of 86.39 mg/g and yield of 31.94 %. The RBBR uptakes response was majorly affected by radiation power and IR whereas MWAC's yield response was significantly affected by radiation power and radiation time. Mechanism analysis divulged that interaction between RBBR molecules and surface functional groups of MWAC was contributed by hydrogen bond, dipole–dipole force, and ion–dipole forces. The adsorption process followed the Freundlich isotherm model which signified multilayer coverage. In terms of kinetic, the adsorption system was best described by PFO. The mass transfer model developed from Polymath can predict the mesopores surface area with high accuracy. Adsorption of RBBR onto MWAC was found to be thermodynamically exothermic, spontaneous in nature, and controlled by physisorption. All in all, MWAC is a good adsorbent for reactive RBBR dye removal.

Funding

This research was funded by the Ministry of Higher Education Malaysia through the Fundamental Research Grant Scheme (project code: FRGS/1/2021/TK0/USM/01/3) and the Postdoctoral Fellowship Scheme from Universiti Sains Malaysia.

Declaration of Competing Interest

The authors declare that they have no known competing financial interests or personal relationships that could have appeared to influence the work reported in this paper.

References

Abbaszadeh, S., Alwi, S.R.W., Webb, C., Ghasemi, N., Muhamad, I. I., 2016. Treatment of lead-contaminated water using activated

carbon adsorbent from locally available papaya peel biowaste. J. Clean. Prod. 118, 210–222.
Ahmad, M.A., Ahmed, N.B., Adegoke, K.A., Bello, O.S., 2021a. Adsorptive potentials of lemongrass leaf for methylene blue dye removal. Chemical Data Collections 31.
Ahmad, A., Rafatullah, M., Sulaiman, O., Ibrahim, M.H., Chii, Y.Y., Siddique, B.M., 2009. Removal of Cu(II) and Pb(II) ions from aqueous solutions by adsorption on sawdust of Meranti wood. Desalination 247, 636–646.
Ahmad, M.A., Yusop, M.F.M., Zakaria, R., Karim, J., Yahaya, N.K. E.M., Mohamed Yusoff, M.A., Hashim, N.H.F., Abdullah, N.S., 2021b. Adsorption of methylene blue from aqueous solution by peanut shell based activated carbon. Mater. Today: Proc. 47, 1246–1251.
Ahmed, M.B., Johir, M.A., Zhou, J.L., Ngo, H.H., Nghiem, L.D., Richardson, C., Moni, M.A., Bryant, M.R., 2019. Activated carbon preparation from biomass feedstock: clean production and carbon dioxide adsorption. J. Clean. Prod. 225, 405–413.
Alberti, G., Amendola, V., Pesavento, M., Biesuz, R., 2012. Beyond the synthesis of novel solid phases: review on modelling of sorption phenomena. Coord. Chem. Rev. 256, 28–45.
Ammendola, P., Raganati, F., Chirone, R., 2017. CO_2 adsorption on a fine activated carbon in a sound assisted fluidized bed: thermodynamics and kinetics. Chem. Eng. J. 322, 302–313.
Asgari, E., Mohammadi, F., Nourmoradi, H., Sheikhmohammadi, A., Rostamifasih, Z., Hashemzadeh, B., Arfaeinia, H., 2022. Heterogeneous catalytic degradation of nonylphenol using persulphate activated by natural pyrite: response surface methodology modelling and optimisation. Int. J. Environ. Anal. Chem. 102, 6041–6060.
Aziz, A., Nasehir Khan, M.N., Mohamad Yusop, M.F., Mohd Johan Jaya, E., Tamar Jaya, M.A., Ahmad, M.A., 2021. Single-Stage microwave-assisted coconut-shell-based activated carbon for removal of Dichlorodiphenyltrichloroethane (DDT) from aqueous solution: optimization and batch studies. Int. J. Chem. Eng. 2021, 9331386.
Azmier, M., Aswareusoff, M., Oladoye, P., Adegoke, K.A., Bell, O., 2021. Optimization and batch studies on adsorption of Methylene blue dye using pomegranate fruit peel based adsorbent. Chem. Data Collect. 32, 100676.
Bazan-Wozniak, A., Nowicki, P., Pietrzak, R., 2017. The influence of activation procedure on the physicochemical and sorption properties of activated carbons prepared from pistachio nutshells for removal of NO_2/H_2S gases and dyes. J. Clean. Prod. 152, 211–222.
Bedin, K.C., de Azevedo, S.P., Leandro, P.K.T., Cazetta, A.L., Almeida, V.C., 2017. Bone char prepared by CO_2 atmosphere: Preparation optimization and adsorption studies of Remazol Brilliant Blue R. J. Clean. Prod. 161, 288–298.
Brazil, T.R., Gonçalves, M., Junior, M.S.O., Rezende, M.C., 2022. Sustainable process to produce activated carbon from Kraft lignin impregnated with H_3PO_4 using microwave pyrolysis. Biomass Bioenergy 156, 106333.
Chen, G., He, S., Shi, G., Ma, Y., Ruan, C., Jin, X., Chen, Q., Liu, X., Dai, H., Chen, X., Huang, D., 2021. In-situ immobilization of ZIF-67 on wood aerogel for effective removal of tetracycline from water. Chem. Eng. J. 423, 130184.
Domergue, L., Cimetière, N., Giraudet, S., Cloirec, P.L., 2022. Adsorption onto granular activated carbons of a mixture of pesticides and their metabolites at trace concentrations in groundwater. J. Environ. Chem. Eng. 10, 108218.
Doumic, L., Salierno, G., Cassanello, M., Haure, P., Ayude, M., 2015. Efficient removal of Orange G using Prussian Blue nanoparticles supported over alumina. Catal. Today 240, 67–72.
Firdaus, M.Y.M., Aziz, A., Azmier Ahmad, M., 2022. Conversion of teak wood waste into microwave-irradiated activated carbon for cationic methylene blue dye removal: optimization and batch studies. Arab. J. Chem. 15, 104081.
Freundlich, H., 1906. Over the adsorption in solution. J. Phys. Chem. 57, 1100–1107.
Ghani, Z.A., Yusoff, M.S., Zaman, N.Q., Zamri, M.F.M.A., Andas, J., 2017. Optimization of preparation conditions for activated carbon from banana pseudo-stem using response surface methodology on removal of color and COD from landfill leachate. Waste Manag. 62, 177–187.
Giri, D.D., Alhazmi, A., Mohammad, A., Haque, S., Srivastava, N., Thakur, V.K., Gupta, V.K., Pal, D.B., 2022. Lead removal from synthetic wastewater by biosorbents prepared from seeds of Artocarpus Heterophyllus and Syzygium Cumini. Chemosphere 287, 132016.
Goswami, R., Kumar Dey, A., 2022. Synthesis and application of treated activated carbon for cationic dye removal from modelled aqueous solution. Arab. J. Chem. 15, 104290.
Ho, Y.S., McKay, G., 1998. Sorption of dye from aqueous solution by peat. Chem. Eng. J. 70, 115–124.
Jabbar, N.M., Salman, S.D., Rashid, I.M., Mahdi, Y.S., 2022. Removal of an anionic Eosin dye from aqueous solution using modified activated carbon prepared from date palm fronds. Chem. Data Collect. 42, 100965.
Jawad, A.H., Saber, S.E.M., Abdulhameed, A.S., Reghioua, A., Alothman, Z.A., Wilson, L.D., 2022. Mesoporous activated carbon from mangosteen (Garcinia mangostana) peels by H3PO4 assisted microwave: Optimization, characterization, and adsorption mechanism for methylene blue dye removal. Diam. Relat. Mater. 129, 109389.
Kishor, R., Purchase, D., Saratale, G.D., Saratale, R.G., Ferreira, L. F.R., Bilal, M., Chandra, R., Bharagava, R.N., 2021. Ecotoxicological and health concerns of persistent coloring pollutants of textile industry wastewater and treatment approaches for environmental safety. J. Environ. Chem. Eng. 9, 105012.
Koble, R.A., Corrigan, T.E., 1952. Adsorption isotherms for pure hydrocarbons. Ind. Eng. Chem. 44, 383–387.
Lagergren, S.K., 1898. About the theory of so-called adsorption of soluble substances. Sven. Vetenskapsakad. Handingarl 24, 1–39.
Langmuir, I., 1918. The adsorption of gases on plane surfaces of glass, mica and platinum. J. Am. Chem. Soc. 40, 1361–1403.
Lellis, B., Fávaro-Polonio, C.Z., Pamphile, J.A., Polonio, J.C., 2019. Effects of textile dyes on health and the environment and bioremediation potential of living organisms. Biotechnol. Res. Innovation 3, 275–290.
Lima, E.C., Hosseini-Bandegharaei, A., Moreno-Piraján, J.C., Anastopoulos, I., 2019. A critical review of the estimation of the thermodynamic parameters on adsorption equilibria. Wrong use of equilibrium constant in the Van't Hoof equation for calculation of thermodynamic parameters of adsorption. J. Mol. Liq. 273, 425–434.
Majd, M.M., Kordzadeh-Kermani, V., Ghalandari, V., Askari, A., Sillanpää, M., 2022. Adsorption isotherm models: a comprehensive and systematic review (2010–2020). Sci. Total Environ. 812, 151334.
McGinley, J., Healy, M.G., Ryan, P.C., Mellander, P.E., Morrison, L., O'Driscoll, J.H., Siggins, A., 2022. Batch adsorption of herbicides from aqueous solution onto diverse reusable materials and granulated activated carbon. J. Environ. Manage. 323, 116102.
Mohammadi, A., Sardar, M., Almasian, M., 2016. Equilibrum and kinetic studies on the adsorption of penicillin G by chestnut shell. Environ. Eng. Manag. J. 15, 167–173.
Mohammadi, A., Nemati, S., Mosaferi, M., Abdollahnejhad, A., Almasian, M., Sheikhmohammadi, A., 2017. Predicting the capability of carboxymethyl cellulose-stabilized iron nanoparticles for the remediation of arsenite from water using the response surface methodology (RSM) model: Modeling and optimization. J. Contam. Hydrol. 203, 85–92.
Motaghi, H., Arabkhani, P., Parvinnia, M., Asfaram, A., 2022. Simultaneous adsorption of cobalt ions, azo dye, and imidacloprid pesticide on the magnetic chitosan/activated carbon@UiO-66 bio-

nanocomposite: Optimization, mechanisms, regeneration, and application. Sep. Purif. Technol. 284, 120258.
Peláez-Cid, A.-A., Herrera-González, A.-M., Salazar-Villanueva, M., Bautista-Hernández, A., 2016. Elimination of textile dyes using activated carbons prepared from vegetable residues and their characterization. J. Environ. Manage. 181, 269–278.
Quesada, H.B., de Araújo, T.P., Cusioli, L.F., de Barros, M.A.S.D., Gomes, R.G., Bergamasco, R., 2022. Caffeine removal by chitosan/activated carbon composite beads: adsorption in tap water and synthetic hospital wastewater. Chem. Eng. Res. Des. 184, 1–12.
Rafatullah, M., Sulaiman, O., Hashim, R., Ahmad, A., 2009. Adsorption of copper (II), chromium (III), nickel (II) and lead (II) ions from aqueous solutions by meranti sawdust. J. Hazard. Mater. 170, 969–977.
Rafatullah, M., Sulaiman, O., Hashim, R., Ahmad, A., 2012. Removal of cadmium (II) from aqueous solutions by adsorption using meranti wood. Wood Sci. Technol. 46, 221–241.
Raj, A., Yadav, A., Rawat, A.P., Singh, A.K., Kumar, S., Pandey, A. K., Sirohi, R., Pandey, A., 2021. Kinetic and thermodynamic investigations of sewage sludge biochar in removal of Remazol Brilliant Blue R dye from aqueous solution and evaluation of residual dyes cytotoxicity. Environ. Technol. Innov. 23, 101556.
Ramutshatsha-Makhwedzha, D., Mavhungu, A., Moropeng, M.L., Mbaya, R., 2022a. Activated carbon derived from waste orange and lemon peels for the adsorption of methyl orange and methylene blue dyes from wastewater. Heliyon, e09930.
Ramutshatsha-Makhwedzha, D., Mavhungu, A., Moropeng, M.L., Mbaya, R., 2022b. Activated carbon derived from waste orange and lemon peels for the adsorption of methyl orange and methylene blue dyes from wastewater. Heliyon 8, e09930.
Rashidi, N.A., Yusup, S., 2017. A review on recent technological advancement in the activated carbon production from oil palm wastes. Chem. Eng. J. 314, 277–290.
Rasoulzadeh, H., Sheikhmohammadi, A., Abtahi, M., Roshan, B., Jokar, R., 2021. Eco-friendly rapid removal of palladium from aqueous solutions using alginate-diatomite magnano composite. J. Environ. Chem. Eng. 9, 105954.
Reddy, Y.S., Rotte, N.K., Hussain, S., Srikanth, V.V., Chandra, M. R., 2023. Sustainable mesoporous graphitic activated carbon as biosorbent for efficient adsorption of acidic and basic dyes from wastewater: Equilibrium, kinetics and thermodynamic studies. J. Hazardous Mater. Adv. 9, 100214.
Rubio-Clemente, A., Gutiérrez, J., Henao, H., Melo, A.M., Pérez, J. F., Chica, E., 2021. Adsorption capacity of the biochar obtained from Pinus patula wood micro-gasification for the treatment of polluted water containing malachite green dye. J. King Saud Univ. – Eng. Sci.
Singh, V.K., Kuma, E.A., 2016. Measurement and analysis of adsorption isotherms of CO_2 on activated carbon. Appl. Therm. Eng. 97, 77–86.
Spessato, L., Bedin, K.C., Cazetta, A.L., Souza, I.P.A.F., Duarte, V. A., Crespo, L.H.S., Silva, M.C., Pontes, R.M., Almeida, V.C., 2019. KOH-super activated carbon from biomass waste: Insights into the paracetamol adsorption mechanism and thermal regeneration cycles. J. Hazard. Mater. 371, 499–505.
Tempkin, M., Pyzhev, V., 1940. Kinetics of ammonia synthesis on promoted iron catalyst. Acta Physicochim. URSS 12, 327.
Tharaneedhar, V., Kumar, P.S., Saravanan, A., Ravikumar, C., Jaikumar, V., 2017. Prediction and interpretation of adsorption parameters for the sequestration of methylene blue dye from aqueous solution using microwave assisted corncob activated carbon. Sustain. Mater. Technol. 11, 1–11.
Vakili, A., Zinatizadeh, A.A., Rahimi, Z., Zinadini, S., Mohammadi, P., Azizi, S., Karami, A., Abdulgader, M., 2023. The impact of activation temperature and time on the characteristics and performance of agricultural waste-based activated carbons for removing dye and residual COD from wastewater. J. Clean. Prod. 382, 134899.
Wan Mahari, W.A., Zainuddin, N.F., Wan Nik, W.M., Chong, C.T., Lam, S.S., 2016. Pyrolysis recovery of waste shipping oil using microwave heating. Energies 9, 780.
Yusop, M.F.M., Aziz, H.A., Ahmad, M.A., 2017. Scavenging remazol brilliant blue R dye using microwave-assisted activated carbon from acacia sawdust: equilibrium and kinetics studies. AIP Conf. Proc., 1892
Yusop, M.F.M., Ahmad, M.A., Rosli, N.A., Gonawan, F.N., Abdullah, S.J., 2021a. Scavenging malachite green dye from aqueous solution using durian peel based activated carbon. Malaysian J. Fundamental Appl. Sci. 17, 95–103.
Yusop, M.F.M., Ahmad, M.A., Rosli, N.A., Manaf, M.E.A., 2021b. Adsorption of cationic methylene blue dye using microwave-assisted activated carbon derived from acacia wood: optimization and batch studies. Arab. J. Chem. 14, 103122.
Yusop, M.F.M., Jaya, E.M.J., Ahmad, M.A., 2022a. Single-stage microwave assisted coconut shell based activated carbon for removal of Zn(II) ions from aqueous solution – Optimization and batch studies. Arab. J. Chem. 15, 104011.
Yusop, M.F.M., Mohd Johan Jaya, E., Mohd Din, A.T., Bello, O.S., Ahmad, M.A., 2022b. Single-Stage optimized microwave-induced activated carbon from coconut shell for cadmium adsorption. Chem. Eng. Technol. 45, 1943–1951.